Available online at www.sciencedirect.com
SCIENCE DIRECT
Journal of Sound and Vibration 293 (2006) 710–727
JOURNAL OF SOUND AND VIBRATION
www.elsevier.com/locate/jsvi

Curve squeal of urban rolling stock—Part 3: Theoretical model

O. Chiello[a,*], J.-B. Ayasse[b], N. Vincent[c], J.-R. Koch[c]

[a]*Laboratoire Transports et Environnement, Institut National de Recherche sur les Transports et leur Securité, 25 avenue François Mitterrand, 69675 Bron cedex, France*
[b]*Laboratoire des Technologies Nouvelles, Institut National de Recherche sur les Transports et leur Securité, 2 avenue du Général Malleret-Joinville, 94114 Arcueil cedex, France*
[c]*VIBRATEC, 28 chemin du petit Bois, 69131 Ecully cedex, France*

Accepted 26 August 2005
Available online 10 March 2006

Abstract

After a brief literature review on friction-induced vibrations and rolling contact, a model of curve squeal generation is presented. Both tangential and normal wheel–rail contact forces as well as axial and radial wheel dynamics are taken into account. For initial conditions close to the quasi-static equilibrium, the squeal occurrence is predicted through the stability analysis of wheel modes (linear analysis). In unstable cases, the squeal level and spectrum are determined through the numerical study of limit cycles in the time-domain (nonlinear analysis). The model is used to study the effect of the friction–velocity relationship and the coupling between tangential and normal dynamics on the stability of the system, especially for large lateral offsets of the wheel–rail contact point. A parameter study is also performed. Results on critical angles of attack, critical wheel damping factors, excited wheel modes and vibration levels are presented. Finally, the results are compared with laboratory and field measurements and the validity of the model is discussed.

1. Introduction

This paper is the last of three companion papers dealing with the curve squeal of rail bound vehicles. Whereas the first two papers have an experimental orientation [1,2] this one focuses on modelling. Since the publication of Rudd's paper in 1976 [3], a lot of curve squeal models have been proposed by researchers [4–17]. However, all of them described the same fundamental mechanism. The angle of attack imposed on the wheels by the bogie dynamics in the curve—the wheel slides laterally across the rail in addition to rolling—is associated with a high lateral "creep-friction" force. This force makes the wheel dynamics unstable, leading to self-excited vibrations and radiated noise. The main differences between the models lie in details in the modelling of wheel/rail mechanical impedances (analytical [4,5,7,10,13–16], FEM [9,11,12,17], with some vertical dynamics added [5,12,17]), contact forces (see Section 2) and wheel sound radiation [9,11,12]. Some authors also studied wheel/rail roughness or wheel rotation effects [10,13,14]. Since the problem is nonlinear, another difference in the models is the method used to predict the long-term dynamic behaviour of the system

*Corresponding author. Tel.: +33 4 72 14 2405.
E-mail address: olivier.chiello@inrets.fr (O. Chiello).

0022-460X/$ - see front matter © 2006 Elsevier Ltd. All rights reserved.
doi:10.1016/j.jsv.2005.12.010

(energy considerations [3], numerical integration [9,11,12,15,16], averaging method [4,5,7,10,13,14]). Some other possible mechanisms have been proposed, like the rubbing of the wheel flanges against the rail or the differential slip between inner and outer wheels on an axle, but they are often dismissed by authors on the basis of Rudd's considerations [3]. Companion papers [1,2] show that they do not represent the main source of noise in a curve.

Despite all these models, the influence of kinetic, mechanical and contact parameters on the occurrence and spectrum of squeal noise is not yet clear. A thorough theoretical parameter study is needed and results have to be compared with experimental observations. This is the main purpose of this paper. It must also be emphasized that the central problem is to predict the vibratory behaviour of the system for a given set of kinetic parameters (rolling speed and angle of attack). Bogie dynamics in the curve and wheel sound radiation can be viewed as secondary problems. In addition, a key parameter in the noise generation is the dynamic modelling of the lateral "creep-friction" force. Indeed, it seems that only a velocity-weakening friction coefficient is able to generate self-excited vibrations, as described by the stick–slip theory. However, other mechanisms of friction-induced vibrations have been reported in the literature and cannot be excluded a priori. So a brief review on friction-induced vibrations and rolling contact has been performed and is presented first.

2. Background

2.1. Friction-induced vibrations

The modelling of dynamic instabilities of mechanical systems with dry friction is a general subject that is widely dealt with in literature (see reviews [18–20]). models with only tangential dynamics (with respect to the contact zone) and models with tangential and normal dynamics may be distinguished. With the former models, only a velocity-weakening of the friction coefficient may lead to instabilities. This weakening can be viewed as a negative damping introduced in the system and has been observed experimentally by many authors. The early works showed that the static friction force could be higher than the kinetic friction force. So, on the basis of the classical Coulomb friction law, two friction coefficients (static and kinetic) may be defined. This distinction is mathematically sufficient to obtain self-excited vibrations in some dynamic systems. Resulting limit cycles are an alternation of sliding and sticking phases, called stick–slip. In addition, the kinetic coefficient may be supposed variable with the relative sliding velocity. In the case of wheel/rail contact, such a variation has been studied by Kraft [21] and has been included in some curve squeal models [9,11,17]. Another distinction level may arise between the quasi-static friction coefficient—for a constant sliding velocity—and the dynamic friction coefficient—when the system is self-excited. A common observation is that the dynamic friction coefficient depends on other parameters than the relative velocity.

For several authors, these distinctions are due to the fact that only tangential dynamics is taken into account in the models. The variation of the friction force would be the consequence of the variation of the normal force, due to normal vibrations of the system [18]. Thus, it has been shown how the coupling of tangential and normal dynamics is sufficient to produce self-excited vibrations with a constant friction coefficient (sprag–slip, mode coupling). This theory has been successfully applied in some squeal problems, especially in the case of braking noises [19,20].

Actually, these two kinds of destabilization may be combined and both have to be explored in each particular situation. In the case of curve squeal noise, most of the existing models take only the tangential (lateral) dynamics into account. However, a recent model reveals a significant effect of the normal (vertical) system dynamics via the lateral position of the contact point on the wheel [17] but this effect needs to be detailed.

2.2. Wheel/rail rolling contact

Tangential rolling contact is characterized by rolling friction which differs from classical dry friction by an important phenomena: for small sliding velocities, the tangential force (creep force) increases linearly with the relative sliding velocity or creepage (which is the ratio of the relative sliding velocity to the rolling velocity)

because of the deformation of the interface during rolling. In addition, three tangent degrees of freedom, lateral, longitudinal and spin, should be rigorously taken into account at the wheel–rail interface. Each of them can be broken down into a quasi-static part imposed by the bogie dynamics and an unknown dynamic part caused by wheel vibrations.

Several rolling contact models have been developed (see reviews [22,23]), rigorous or simplified, linear or nonlinear, steady state or non-steady state. For curve squeal, a nonlinear model is needed because the sliding velocities are significant. moreover, a non-steady-state model would be desirable since frequencies at which squeal occurs correspond to wavelengths generally smaller than the contact zone. Unfortunately, today, the only nonlinear and non-steady-state existing model (e.g. CONTACT software, see Ref. [22]) provides computational performances which are too lengthy to be used in such an application [23]. Several authors, especially in the problem of squeal noise, carried out the inclusion of a velocity-weakening friction coefficient in rolling contact models. Analytical formulae are frequently used [11,17] (e.g. the heuristic association of the Vermulen-Johnson model with the Kraft expression of the friction coefficient) but some authors modified numerical contact models, notably the FASTSIM software [12].

3. Description of the model

3.1. Statement of the problem

A loaded wheel with constant rolling speed V_x and angle of attack α is considered (see Fig. 1). The resulting sliding velocity is noted $V_y \simeq \alpha V_x$. Dynamic vertical and lateral wheel displacements at the wheel–rail contact point are noted, respectively, u_z and u_y in a Cartesian reference system moving with the wheel. $v_y = \partial u_y/\partial t$ denotes the dynamic lateral contact velocity and ξ_y is the so-called dynamic lateral creepage defined by

$$\xi_y = \frac{V_y - v_y}{V_x} \simeq \alpha - \frac{v_y}{V_x}. \tag{1}$$

Wheel rotation and wheel/rail surface irregularities are neglected. The rail is assumed to be rigid, apart from the contact zone.

3.2. Wheel dynamics

The dynamic behaviour of the wheel is assumed to be linear and lightly damped so that a real modal basis can be used. This basis is presumed to be known in the frequency range of interest. A mode i is characterized

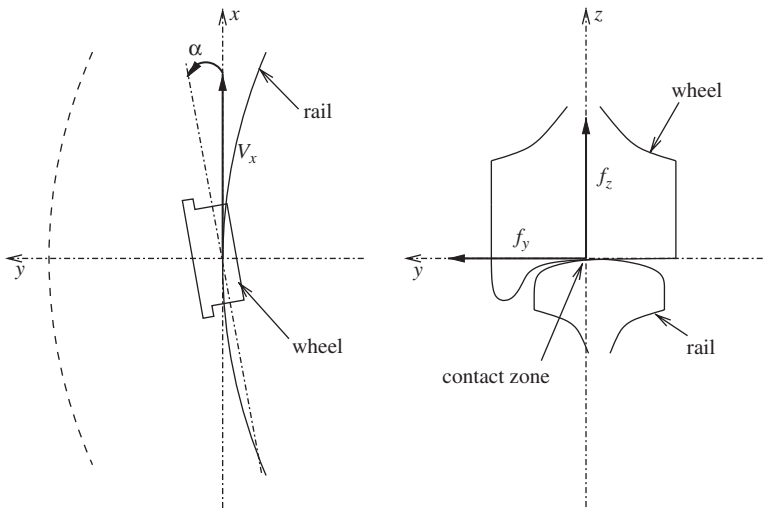

Fig. 1. Coordinate system, kinetic variables and applied forces.

by its natural circular frequency ω_i, its vertical and lateral modal amplitudes at the contact point Φ_{zi} and Φ_{yi} (assumed to be normalized with respect to mass) and its structural damping factor η_i. Two kinds of mode may be distinguished: the radial modes Rn and the axial modes mLn, where n is the number of nodal diameters and m is the number of nodal circles. At the contact point, wheel vertical and lateral displacements can be written as

$$u_z = \mathbf{\Phi}_z \mathbf{w}, \tag{2}$$

$$u_y = \mathbf{\Phi}_y \mathbf{w}, \tag{3}$$

where $\mathbf{\Phi}_z$ and $\mathbf{\Phi}_y$ are the vectors of vertical and lateral modal amplitudes at the contact point and $\mathbf{w}$ denotes the unknown generalized coordinates vector.

3.3. Contact forces

A nonlinear Hertzian dynamic vertical force $f_z(u_z)$ is assumed, given by

$$f_z = N\left(\frac{\delta_s - u_z}{\delta_s}\right)^{3/2}, \tag{4}$$

where δ_s denotes the static wheel/rail penetration caused by the vertical wheel load N (see Appendix A). Spin and longitudinal creep forces are neglected. A dynamic lateral "creep-friction" force $f_y(f_z, \xi_y)$ is assumed by using a nonlinear exponential creep model (see Refs. [22,24]) combined with a dynamic friction coefficient μ decreasing linearly with the relative contact velocity:

$$f_y = \mu f_z\left(1 - \mathrm{e}^{-\bar{\xi}_y}\right)\mathrm{sgn}(\xi_y), \tag{5}$$

$$\bar{\xi}_y = \frac{1}{\mu f_z} G a_1 b_1 C_{22} f_z^{2/3} |\xi_y|, \tag{6}$$

$$\mu = \mu_s + \gamma |V_y - v_y| = \mu_s + \gamma V_x |\xi_y|, \tag{7}$$

where G denotes the mean shear modulus of the materials in contact, a_1 and b_1 the normalized semi-axis lengths of the contact ellipse and C_{22} the Kalker coefficient (see Appendix A). A key parameter is the slope of the friction coefficient with the relative contact velocity $\gamma \leqslant 0$. The case $\gamma = 0$ corresponds to a constant friction coefficient. Figs. 2 and 3 show the variation of f_y with ξ_y and v_y for a given vertical force f_z. Two zones can be distinguished, separated by a critical creepage α_c, corresponding to a critical wheel vibratory velocity $v_{yc} = V_x(\alpha - \alpha_c)$:

- for small creepages, f_y increases linearly with ξ_y (linear creep theory),
- for large creepages, f_y is saturated (dry friction theory) but decreases linearly with ξ_y because of the velocity-weakening friction coefficient.

At the quasi-static equilibrium, the vertical displacement u_z and the lateral velocity v_y are zero. The vertical contact force f_z is then equal to the static wheel load N and the lateral creepage ξ_y is equal to the angle of attack α. The corresponding quasi-static "creep-friction" force is denoted T_y such that

$$T_y = f_y|_{f_z = N,\ \xi_y = \alpha}. \tag{8}$$

It must be emphasized that with this model, the quasi-static and dynamic variations $T_y(\alpha)$ and $f_y(\xi_y)$ are the same.

3.4. Wheel excitation

Modal expansion of the non-stationary part of the wheel dynamics leads to the following system of equations:

$$\frac{\partial^2 \mathbf{w}}{\partial t^2} + 2\mathbf{\Xi\Omega}\frac{\partial \mathbf{w}}{\partial t} + \mathbf{\Omega}^2 \mathbf{w} = \mathbf{\Phi}_z^{\mathrm{T}}(f_z - N) + \mathbf{\Phi}_y^{\mathrm{T}}(f_y - T_y), \tag{9}$$

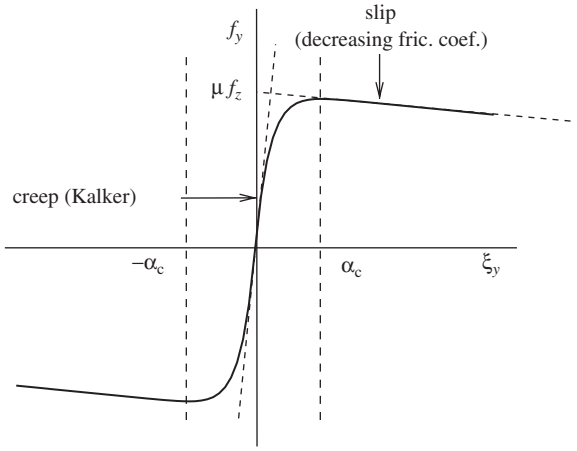

Fig. 2. "Creep-friction" force f_y as a function of the dynamic lateral creepage ξ_y.

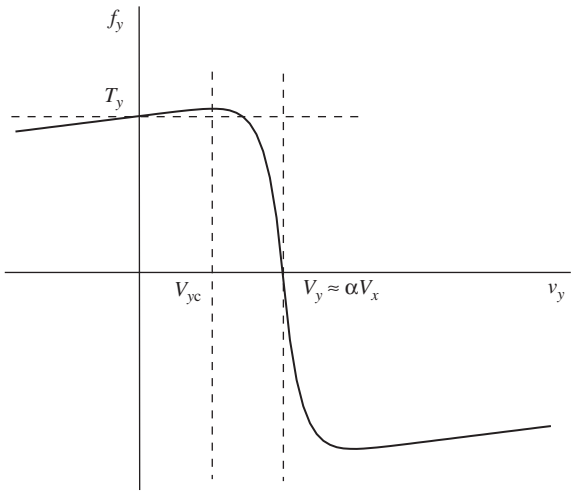

Fig. 3. "Creep-friction" force f_y as a function of the lateral wheel velocity v_y.

where $\mathbf{\Omega}$ denotes the diagonal matrix of natural frequencies ω_i and $\mathbf{\Xi}$ the diagonal matrix of viscous modal damping factors $\xi_i = \eta_i/2$. Together with the expression of contact forces and contact coordinates (1)–(8), Eq. (9) represents a system of second-order nonlinear differential equations with an equilibrium point $\mathbf{w} = \partial\mathbf{w}/\partial t = \mathbf{0}$. If initial conditions are different from this point, two cases may be distinguished:

- the stable (non-squealing) case if the solution converges to the equilibrium,
- the unstable (squealing) case if the solution converges to a periodic, quasi-periodic or chaotic limit cycle.

Time-domain solutions are obtained by numerical integration of the system.

3.5. Stability analysis

For initial conditions sufficiently close to the equilibrium, a linear stability analysis can be performed. Linearizing the contact forces around quasi-static values N and T_y, system (9) becomes:

$$\frac{\partial^2\mathbf{w}}{\partial t^2} + \left(2\mathbf{\Xi\Omega} + \mathbf{\Phi}_y^{\mathrm{T}} c_{yy} \mathbf{\Phi}_y\right) \frac{\partial\mathbf{w}}{\partial t} + \left(\mathbf{\Omega}^2 + \mathbf{\Phi}_z^{\mathrm{T}} k_{zz} \mathbf{\Phi}_z + \mathbf{\Phi}_y^{\mathrm{T}} k_{yz} \mathbf{\Phi}_z\right)\mathbf{w} = \mathbf{0}, \tag{10}$$

where k_{zz}, c_{yy} and k_{yz} are, respectively, the vertical Hertzian stiffness, the lateral viscous damping and the vertical/lateral cross-stiffness at the contact point given by

$$k_{zz} = -\left.\frac{\partial f_z}{\partial u_z}\right|_{u_z=0}, \tag{11}$$

$$c_{yy} = -\left.\frac{\partial f_y}{\partial v_y}\right|_{u_z=0,\ v_y=0}, \tag{12}$$

$$k_{yz} = -\left.\frac{\partial f_y}{\partial u_z}\right|_{u_z=0,\ v_y=0}. \tag{13}$$

Thus, two factors of instability coexist:

- a negative lateral contact damping $c_{yy} \simeq \gamma N$ when $\alpha > \alpha_c$ and $\gamma < 0$ due to the velocity-weakening friction coefficient (negative damping instability)
- a stiffness matrix asymmetry induced by cross-stiffness k_{yz} (mode coupling instability).

The stability may be deduced from a complex eigenvalue analysis of system (10). For a complex mode i with complex eigenvalue λ_i, $\Re(\lambda_i)$ represents its growth rate. The mode is then unstable if and only if $\Re(\lambda_i)$ is positive. Modal growth rates can be expressed in dB/s by using the indicator $\Delta_i = 10\Re(\lambda_i)/\ln 10$.

3.6. Approximate stability criterion

Neglecting mode coupling (non-diagonal terms), leads to an approximate expression of growth rates:

$$\Re(\lambda_i) \simeq -\tfrac{1}{2}(\eta_i\omega_i + \Phi_{yi}^2 c_{yy}) \simeq \tfrac{1}{2}(|\gamma| N\Phi_{yi}^2 - \eta_i\omega_i) \quad \text{for } \alpha > \alpha_c. \tag{14}$$

This allows one to define an approximate critical damping factor:

$$\eta_{ci} = \frac{|\gamma| N\Phi_{yi}^2}{\omega_i} \tag{15}$$

under which the mode is unstable. According to this criterion and for a lightly damped wheel, axial modes with no nodal circle (0Ln) and $n > 1$ are generally all unstable for $\alpha > \alpha_c$, even for small γ values, since their lateral modal amplitudes are large and their damping factors are small (see Section 4.1). The approximate critical damping factors are inversely proportional to the natural frequencies of the modes so that the mode with the largest growth factor is generally one of the low or medium-order modes ($1 < n < 5$). However, this stability criterion (similar to the criterion given by Heckl [16]) does not take into account any lateral/vertical coupling.

4. Numerical results

4.1. General points

Both stability analysis and time-domain integration have been performed for a monobloc metro wheel (diameter 0.85 m, mass 332 kg, straight web, web thickness 0.022 m). Radial and axial modes in the range 0–6000 Hz have been determined from a finite element model of the wheel. Modal amplitudes $\mathbf{\Phi}_z$ have been calculated as a function of an optional offset u_{y+} of the lateral contact point position on the wheel. For $u_{y+} = 0$, the distance between the point of contact and the internal face of the tyre is 0.07 m. All modal damping factors have been set to 0.01% except those of the low-order modes ($n = 0, 1$) for which a damping factor of 1% has been chosen to simulate the axle damping effect. Table 1 summarizes the values of kinetic and contact parameters used in the parameter study. The central column is the reference configuration.

A first parameter study based on the approximate stability criterion has been performed (see Tables 2–4). The range of the critical angle of attack is found to vary from 9 to 16 mrad with a significant effect of all parameters and a value of 13.2 mrad in the reference configuration. The approximate critical damping factors of 0Ln modes are always greater than 0.01% even for small values of γN. So 0Ln modes with $n>1$ are always unstable after the critical angle of attack and negative damping instabilities may occur. In addition, approximate modal growth rates are rather similar for these modes with a small advantage to 0L2, 0L3 and 0L4 modes, according to γ.

4.2. Validity of the approximate stability criterion

In order to evaluate the validity domain of the approximate stability criterion, the modal growth rates of 0Ln modes have been calculated by using different approximations and for different lateral offsets of the

Table 1
Range of kinetic and contact parameters used in the parameter study

Parameter	Unit	Minimum value	Reference value	Maximum value
α	mrad	15	20	25
V_x	km/h	10	20	40
u_{y+}	m	−0.02	0	+0.02
N	kN	25	45	62.5
μ_s	—	0.3	0.4	0.5
$\lvert\gamma\rvert = -\gamma$	s/m	0.05	0.1	0.5

Table 2
Variation of the critical angle of attack with the parameters

Configuration	α_c (mrad)
Reference	13.2
V_x min.	14.9
V_x max.	11.5
N min.	11.3
N max.	14.5
μ_s min.	9.9
μ_s max.	16.6
$\lvert\gamma\rvert$ min.	14.9
$\lvert\gamma\rvert$ max.	9.2

Table 3
Variation of the approximate critical damping factors of 0Ln modes with the parameters

Mode	$f_i = \omega_i/2\pi$ (Hz)	η_{ci} (%)		
		$\lvert\gamma\rvert N$ min.	Reference	$\lvert\gamma\rvert N$ max.
0L0	326	0.31	1.12	7.80
0L1	239	0.92	3.31	22.96
0L2	447	0.53	1.91	13.24
0L3	1154	0.21	0.76	5.28
0L4	2058	0.12	0.43	2.98
0L5	3066	0.08	0.29	1.98
0L6	4130	0.06	0.21	1.44
0L7	5222	0.04	0.16	1.10

Table 4
Variation of the approximate modal growth rates of 0Ln modes with the parameters

Config.	Δ_i (dB/s)							
	0L0	0L1	0L2	0L3	0L4	0L5	0L6	0L7
Ref.	3.0	69.9	109.9	*112.2*	111.6	109.2	105.2	99.7
α min.	−17.5	25.6	62.2	*63.0*	62.1	60.2	57.3	53.5
α max.	5.2	74.7	115.1	*117.5*	116.9	114.4	110.3	104.7
V_x min.	−0.0	63.4	102.9	*104.9*	104.3	101.9	98.1	92.9
V_x max.	4.5	73.1	113.4	*115.7*	115.1	112.7	108.6	103.0
N min.	−17.0	26.8	63.4	*64.3*	63.4	61.5	58.5	54.7
N max.	17.3	100.7	143.1	*146.3*	145.9	143.2	138.4	131.8
μ_s min.	5.4	75.0	115.4	*117.8*	117.2	114.8	110.6	105.0
μ_s max.	−9.3	43.4	81.3	*82.7*	82.0	79.8	76.5	72.1
$\|\gamma\|$ min.	−30.1	−3.2	*31.0*	30.9	29.9	28.3	26.1	23.5
$\|\gamma\|$ max.	204.5	504.6	578.7	594.6	*596.6*	589.8	575.0	552.8

Mode in italics has largest growth rate.

Table 5
Growth rates of 0Ln modes (a) (b) with mode coupling but no vertical dynamics ($k_{zz} = k_{yz} = 0$), (c) with mode coupling and vertical dynamics

Config.	Approx.	Δ_i (dB/s)							
		0L0	0L1	0L2	0L3	0L4	0L5	0L6	0L7
Ref.	(a)	3.0	69.9	109.9	*112.2*	111.6	109.1	105.2	99.7
Ref.	(b)	3.0	70.0	109.9	112.2	*112.3*	109.2	105.2	100.0
Ref.	(c)	2.9	71.3	109.7	112.6	*114.9*	110.2	107.2	105.3
u_{y+} min.	(c)	0.9	96.0	95.1	111.3	*117.5*	108.8	105.9	102.2
u_{y+} max.	(c)	3.1	41.9	*124.8*	112.1	100.6	112.8	107.0	108.4

Mode in italics has largest growth rate.

contact point (see Table 5 and Fig. 4). From these results, it can be concluded that the mode coupling effect is significant only if the vertical dynamics is present. In addition, this effect is important only for large lateral offsets, which can be explained by the induced vertical/lateral coupling. However, it is important to note that a lateral offset is not found to stabilize or destabilize a mode: it only changes the mode having the largest growth rate. This assumption is corroborated by the fact that, in the $\gamma = 0$ case (constant friction coefficient), no mode coupling instability occurs even for large lateral offsets (see Fig. 5). In Appendix B, some elements are presented which may explain why these results are different from those given in Ref. [17]. As a conclusion, the approximate stability criterion can be used to determine if a mode is stable or unstable but not to evaluate the relative degrees of instability.

4.3. Times histories

Time-domain solutions are now discussed for the reference configuration and without vertical dynamics ($f_z = N$). The initial conditions are set so that the initial displacements are zero, the initial lateral velocity represents 10% of the sliding velocity V_y and the contributions of 0Ln modes are all the same. Figs. 6, 7 and 8, respectively, show the time histories of the lateral wheel velocity v_y, the instantaneous "creep-friction" coefficient f_y/N and the modal contributions to the short time average level of the lateral velocity v_y. Three

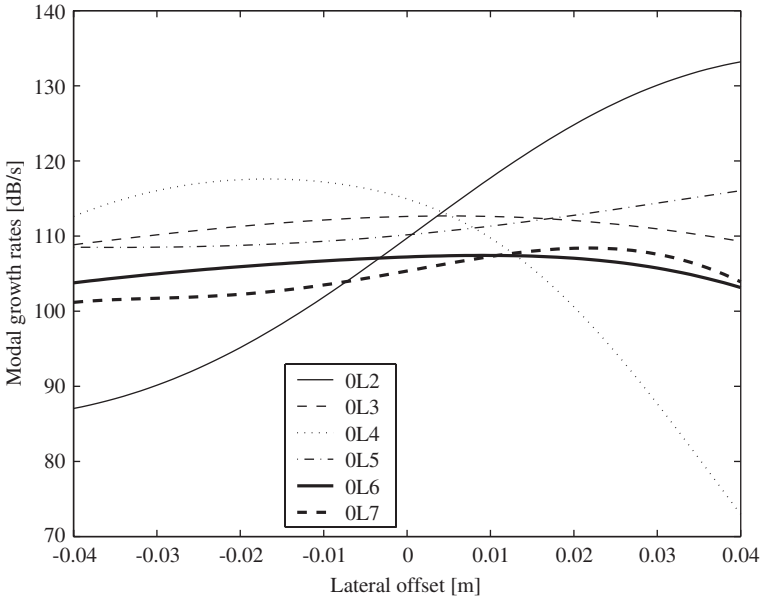

Fig. 4. Variation of the growth rates of 0Ln modes with the lateral offset u_{y+} for reference configuration.

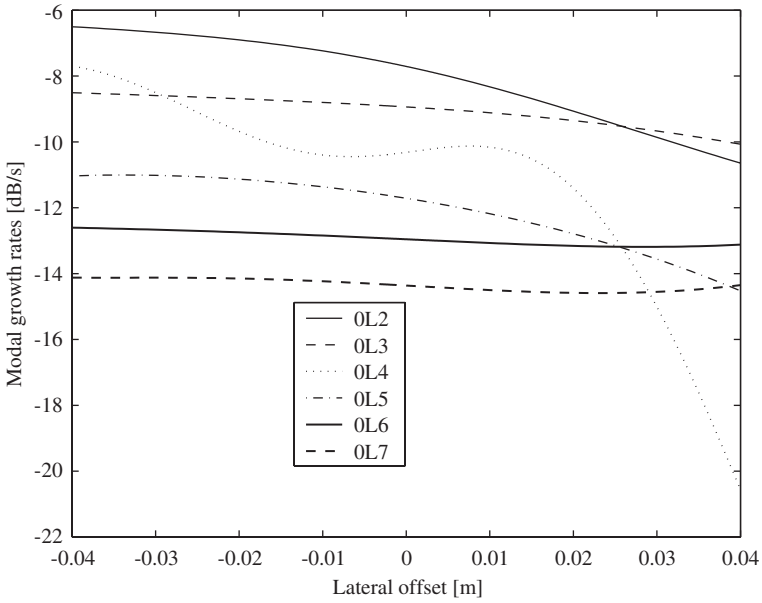

Fig. 5. Variation of the growth rates of 0Ln modes with the lateral offset u_{y+} for reference configuration but $\gamma = 0$ (constant friction coefficient).

phases may be distinguished:

(1) the wheel contact point slides and the contact damping is negative; the lateral velocity increases with modal contributions given by the modal growth rates until it reaches the critical velocity $v_{yc} \simeq 0.038\,\mathrm{m/s}$,
(2) the wheel contact point begins to creep and the contact damping is positive in some phases of the oscillation which slows down the growth of the lateral velocity; the unstable modes are in competition until the mode 0L3 emerges and becomes dominant (mode lock-in),

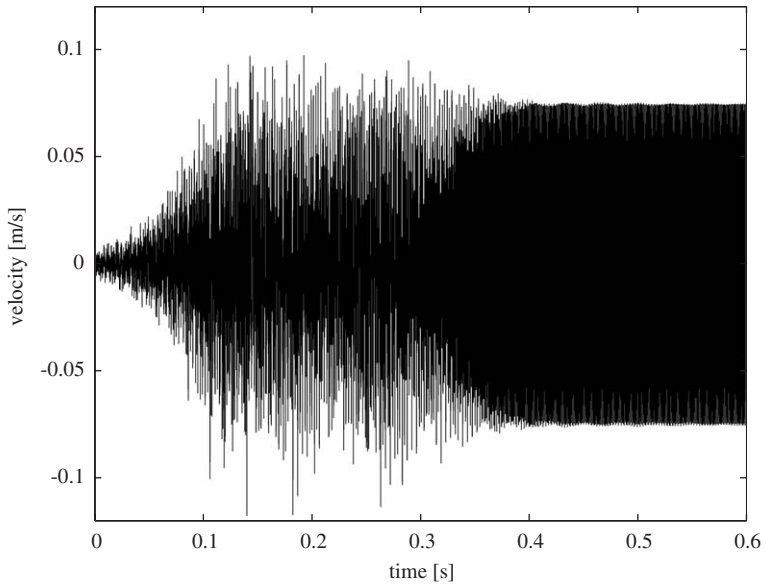

Fig. 6. Time history of the lateral wheel velocity v_y for reference configuration.

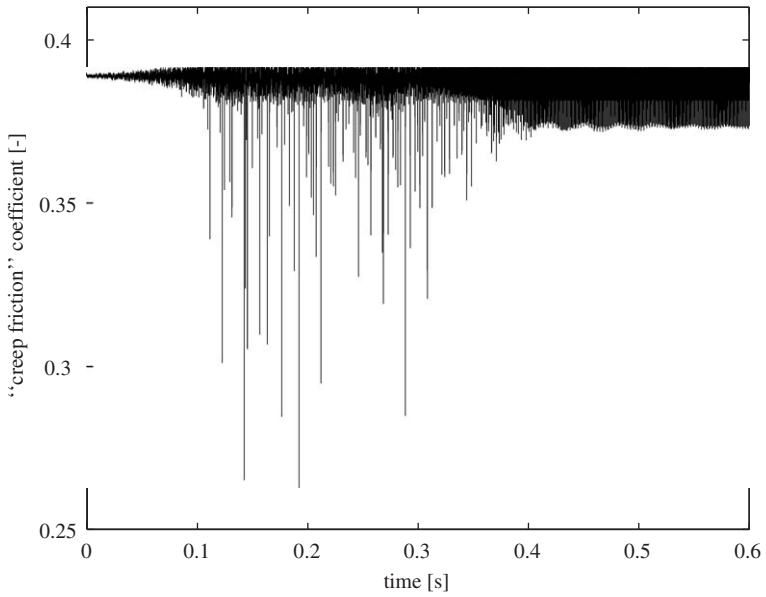

Fig. 7. Time history of the instantaneous "creep-friction" coefficient f_y/N for reference configuration.

(3) the lateral velocity stabilizes between the critical velocity v_{yc} and the sliding velocity $V_y \simeq 0.11\,\mathrm{m/s}$; the solution converges to a periodic creep–slip limit cycle.

With similar modal initial contributions, the dominant mode is generally the one with the largest growth rate but it may also be a mode with an inferior order which has sufficiently large growth rate (like 0L3 in the current example). Anyway, it can be shown that the dominant mode is strongly influenced by the initial conditions (see Section 4.5 for instance), which are actually unknown because they depend on other parameters (e.g. surface irregularities or angle variation in the curve).

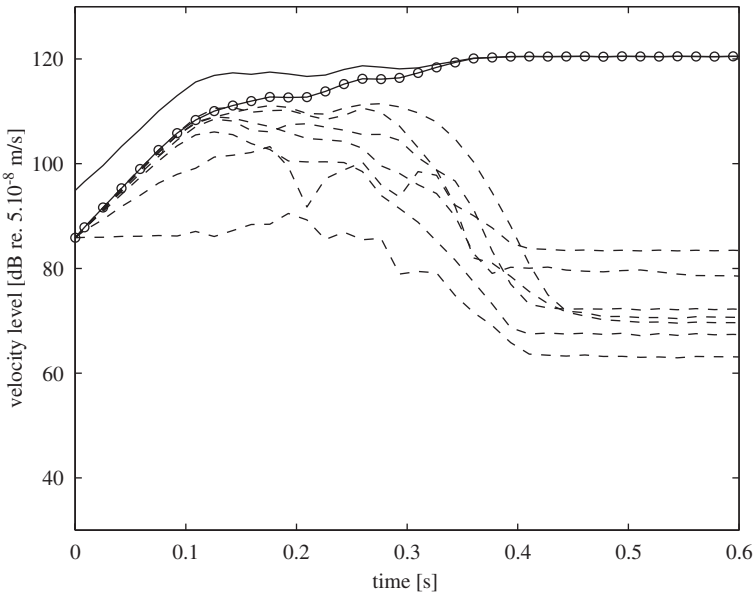

Fig. 8. Time history of the short time average level of the lateral wheel velocity v_y (solid line), contribution of the 0L3 mode (solid line with circles), contributions of other 0Ln modes (dashed lines) for reference configuration.

4.4. Properties of the limit cycles

Fig. 9 shows the combined variations of v_y and f_y/N in the limit cycle obtained after 1.5 s. The creep and slip stages can be easily identified. The fundamental frequency of the cycle is very close to the natural frequency of the dominant mode 0L3 (1154 Hz). As shown in Fig. 10, some harmonics (more than 35 dB below the peak) remain because of the system nonlinearity.

An interesting observation is that the average "creep-friction" force in the limit cycle is slightly lower (−1%) than the quasi-static "creep-friction" force T_y. This implies that the self-excited vibrations decrease the average friction coefficient a little further.

4.5. Case of harmonically-related modes

Figs. 11 and 12 show the case where the mode 0L4 is favoured by an important initial contribution. In this case, both modes 0L4 and 0L6 can coexist in the limit cycle because they are harmonically related. Indeed, their respective natural frequencies are 2058 and 4130 Hz. This has already been observed by Heckl [16,15] and Nakai et al. [5].

5. Correlation with experimental results

Results of the parameter study have been compared with the experimental results reported in companion papers [1,2]. In order to facilitate this comparison, qualitative theoretical effects of parameters have been summarized in Table 6.

First, the measured spectra are very similar to theoretical predictions in terms of squealing modes (0L2, 0L3 and 0L4), vibratory amplitudes and harmonics. In particular, the sliding velocity $V_y \simeq \alpha V_x$ seems to be a good estimation of the wheel contact velocity during squeal, which is a characteristic of the creep–slip limit cycles given by the model. As already mentioned, the prediction of the order n of the squealing 0Ln mode is delicate, due to the uncertainty of initial conditions. However, some theoretical tendencies are confirmed by experience (for instance higher orders in the case of higher rolling speeds).

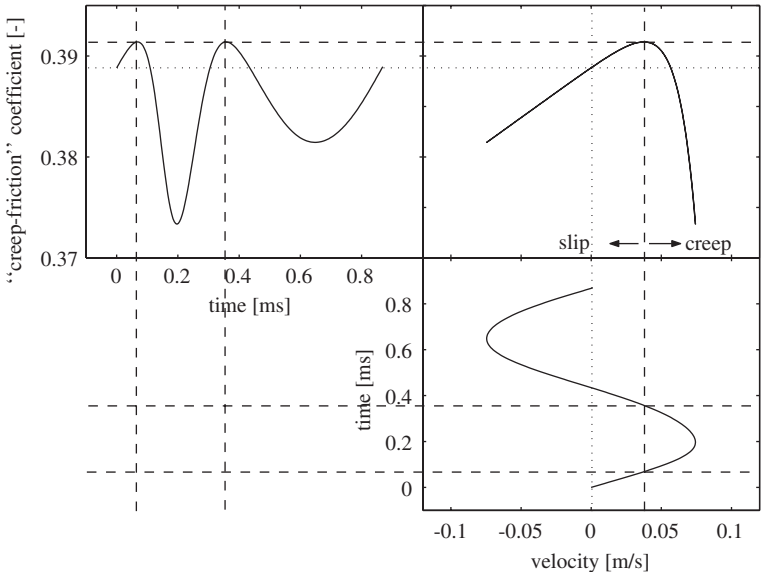

Fig. 9. Combined variations of the contact lateral velocity v_y and the "creep-friction" coefficient f_y/N in the limit cycle for reference configuration.

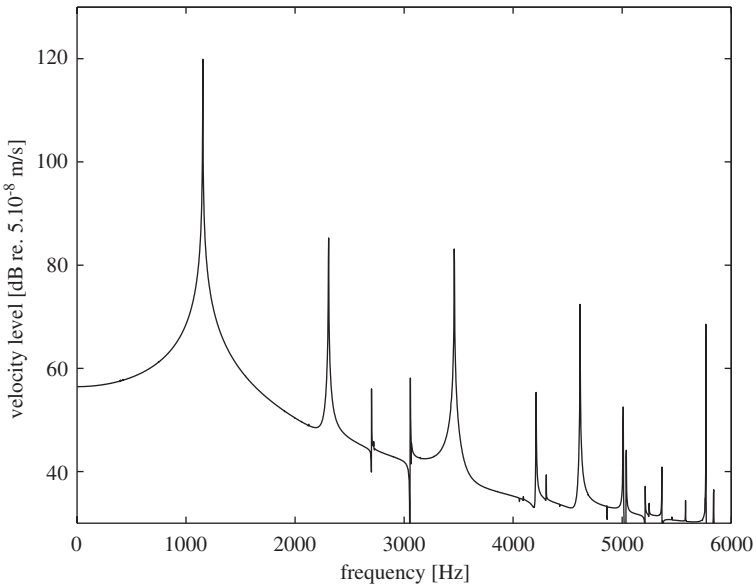

Fig. 10. Power spectrum of the lateral wheel velocity v_y after stabilization for reference configuration.

The correlations in terms of the critical angles of attack and critical damping factors, which are the key parameters in squeal occurrence, are encouraging, on the condition that a correct value for the friction coefficient slope γ is chosen. With $\gamma = -0.1$ s/m (the chosen value in the previous reference configuration), a critical damping factor around 2% for the 0L2 mode can be obtained in a configuration simulating the $\frac{1}{4}$ scale rig described in Ref. [2]. This agrees well with the 1–3% range of critical damping factors founded experimentally. Unfortunately, contrary to most publications dealing with curve squeal, the decrease of the average "creep-friction" force at high angles of attack has not been observed experimentally. Consequently, it

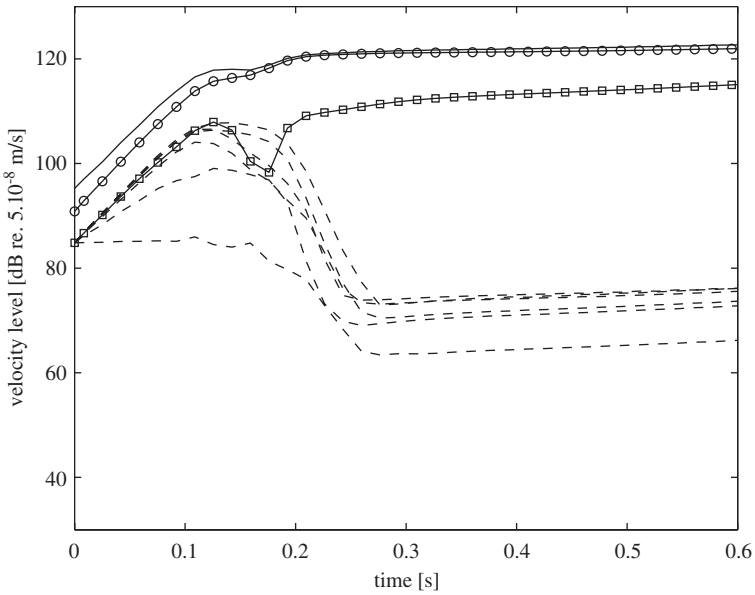

Fig. 11. Case of harmonically related modes—time history of the short time level of the lateral wheel velocity v_y (solid line), contribution of the 0L4 mode (solid line with circles), contribution of the 0L6 mode (solid line with squares), contributions of other 0Ln modes (dashed lines).

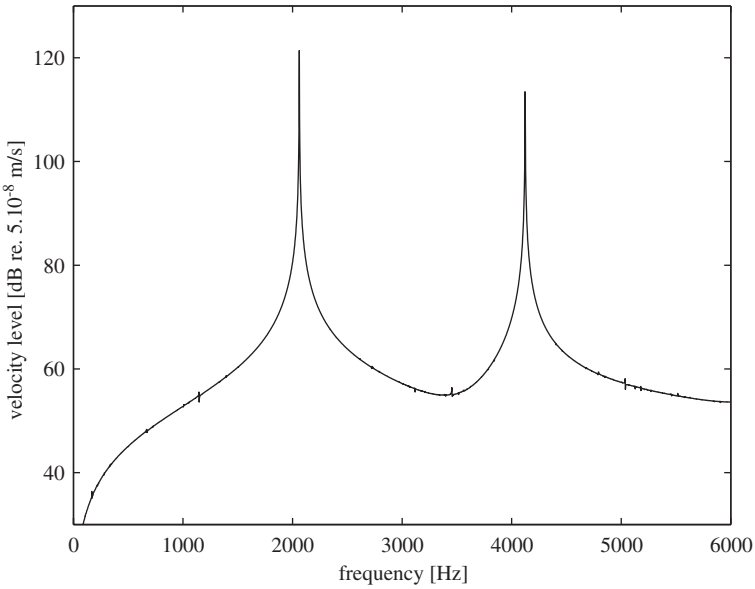

Fig. 12. Case of harmonically related modes—power spectrum of the lateral wheel velocity v_y after stabilization.

has not been possible to identify the value of the slope γ. This is the main limitation of this validation. A hypothesis is that the instantaneous friction coefficient decreases with contact velocity whereas the average friction coefficient remains constant with the angle of attack. This hypothesis could be confirmed by measuring the instantaneous ''creep-friction'' force and by using a more realistic modelling (e.g. a non-steady-state model) of this force.

Table 6
Qualitative theoretical effects of the parameters on squeal (general tendencies)

Parameter	Occurrence		Properties	
	Critical angle of attack α_c	Critical damping factors η_{ci}	Order n of the squealing mode 0Ln	Noise level
α		+	+	++
V_x	−	+	+	++
u_{y+}		+/−	++/−−	
N	+	++	++	−
μ_s	++	−	−	−
$\lvert\gamma\rvert = -\gamma$	−−	++	++	+

6. Conclusion

A model of curve squeal generation has been presented. Compared with existing models, the main originalities are the inclusion of vertical dynamics and the possible determination of both modal growth rates (squeal occurrence) and limit cycles (squeal level and spectrum). The correlation with experimental results is rather satisfactory, especially in terms of vibratory levels. Despite an observed coupling of lateral and vertical dynamics, in particular for large offsets of the lateral contact position on the wheel, numerical results show that only a velocity-weakening friction coefficient is able to destabilize the system and induce wheel vibrations. However, the measurement of the corresponding slope is difficult and a fine prediction of squeal occurrence remains delicate without supplementary research on the transient nature of the frictional rolling contact.

Acknowledgements

This work is part of a French research project concerned with the curve squeal reduction of urban railway rolling stock. The authors wish to acknowledge the French Ministry of Research for its financial support and all other project partners, RATP, ALSTOM and VALDUNES.

Appendix A. Calculation of the contact parameters

Assuming a Hertzian contact (see Ref. [25]), the static wheel/rail penetration caused by a static vertical load N, is given by

$$\delta_s = r\left(\left(\frac{3}{2}N\frac{1-\nu^2}{E}\right)^2(A+B)\right)^{1/3}, \tag{A.1}$$

where r is a coefficient that is a function of the angle θ such that:

$$\cos\theta = \frac{|B-A|}{B+A} \tag{A.2}$$

and

$$A = \frac{1}{2}\left(\frac{1}{R_{xx\mathrm{w}}} + \frac{1}{R_{xx\mathrm{r}}}\right), \tag{A.3}$$

$$B = \frac{1}{2}\left(\frac{1}{R_{yy\mathrm{w}}} + \frac{1}{R_{yy\mathrm{r}}}\right). \tag{A.4}$$

In these equations, $R_{xx\mathrm{w}}$, $R_{yy\mathrm{w}}$, $R_{xx\mathrm{r}}$ and $R_{yy\mathrm{r}}$ denote, respectively, the longitudinal and transverse wheel and rail radii of curvature at the contact point and E, ν and $G = E/2(1-\nu^2)$ denote, respectively, the mean Young

modulus, the Poisson ratio and the shear modulus of the materials in contact. In addition, the product $a_1 b_1$ of the normalized semi-axis of the contact ellipse can be written as

$$a_1 b_1 = mn\left(\frac{3}{2}\frac{1-\nu^2}{E}(A+B)\right)^{2/3}, \tag{A.5}$$

where m and n are also functions of the angle θ. Finally, the Kalker coefficient C_{22} corresponding to the lateral creepage depends on the ratio $g = b_1/a_1 = n/m$ and on the Poisson ratio. Coefficients r, m, n and g are calculated using a polynomial interpolation of the values given by Hertz (see Ref. [25]) whereas C_{22} is calculated using an interpolation of the values given by Kalker for Poisson ratios of 0, 0.25 and 0.5 (see Ref. [22]).

Appendix B. Effect of the lateral contact position on wheel modes stability: formulation in the frequency domain

B.1. Nyquist criterion and stability

By assuming a harmonic dependance for all dynamic variables X such that $X = \Re(\hat{X}(\omega)\exp(\mathrm{j}\omega t))$, the linearized equations of the system become:

$$(-\omega^2\mathbf{I} + 2j\omega\boldsymbol{\Xi}\boldsymbol{\Omega} + \boldsymbol{\Omega}^2)\hat{\mathbf{q}} = \boldsymbol{\Phi}_y^{\mathrm{T}}\hat{f}_y + \boldsymbol{\Phi}_z^{\mathrm{T}}\hat{f}_z, \tag{B.1}$$

$$\hat{u}_z = \boldsymbol{\Phi}_z\hat{\mathbf{q}}, \tag{B.2}$$

$$\hat{v}_y = \mathrm{j}\omega\boldsymbol{\Phi}_y\hat{\mathbf{q}}, \tag{B.3}$$

$$\hat{f}_z = -k_{zz}\hat{u}_z, \tag{B.4}$$

$$\hat{f}_y = \frac{k_{yz}}{k_{zz}}\hat{f}_z - c_{yy}\hat{v}_y. \tag{B.5}$$

These equations lead to a loop gain for the lateral contact force $\hat{f}_y$:

$$\hat{f}_y = H_1\hat{f}_y + H_2\hat{f}_y = H\hat{f}_y, \tag{B.6}$$

with

$$H_1 = \frac{k_{yz}}{k_{zz}}\frac{\hat{f}_z}{\hat{f}_y} = \frac{k_{yz}}{k_{zz}}\left(\frac{-H_{yz}}{H_{zz} + (\mathrm{j}\omega/k_{zz})}\right), \tag{B.7}$$

$$H_2 = -c_{yy}\frac{\hat{v}_y}{\hat{f}_y} = c_{yy}\left(\frac{H_{yz}^2}{H_{zz} + (\mathrm{j}\omega/k_{zz})} - H_{yy}\right), \tag{B.8}$$

$$\begin{bmatrix} H_{yy} & H_{yz} \\ H_{yz} & H_{zz} \end{bmatrix} = \mathrm{j}\omega\begin{bmatrix} \boldsymbol{\Phi}_y \\ \boldsymbol{\Phi}_z \end{bmatrix}(-\omega^2\mathbf{I} + 2\mathrm{j}\omega\boldsymbol{\Xi}\boldsymbol{\Omega} + \boldsymbol{\Omega}^2)^{-1}\begin{bmatrix} \boldsymbol{\Phi}_y \\ \boldsymbol{\Phi}_z \end{bmatrix}^{\mathrm{T}}, \tag{B.9}$$

where H_{yy}, H_{zz} and H_{yz} are the lateral, vertical and cross-mobility of the wheel at the contact point.

As in Ref. [17], the instability of the system can be determined by the Nyquist criterion, which states that the system is unstable for frequencies where the Nyquist contour H passes the real axis at the right-hand side of 1 ($\Re(H) > 1$ and $\Im(H) = 0$). It can be shown that instabilities may occur *near* the frequencies of the axial wheel modes, especially those with no nodal circles. The case of the mode with 2 nodal diameters (0L2) is studied here for the reference configuration. Its natural circular frequency is noted ω_{02}.

B.2. Loop gain at the natural frequency of the mode

The variations of the real parts of the transfer functions $H(\omega_{02})$, $H_1(\omega_{02})$ and $H_2(\omega_{02})$ with the lateral offset u_{y+} are given in Fig. 13. These results are rather similar than those given in Ref. [17]. In particular, $\Re(H_1)$ changes polarity. As a result, $\Re(H)<1$ for some lateral offsets, which might be interpreted as a stabilization.

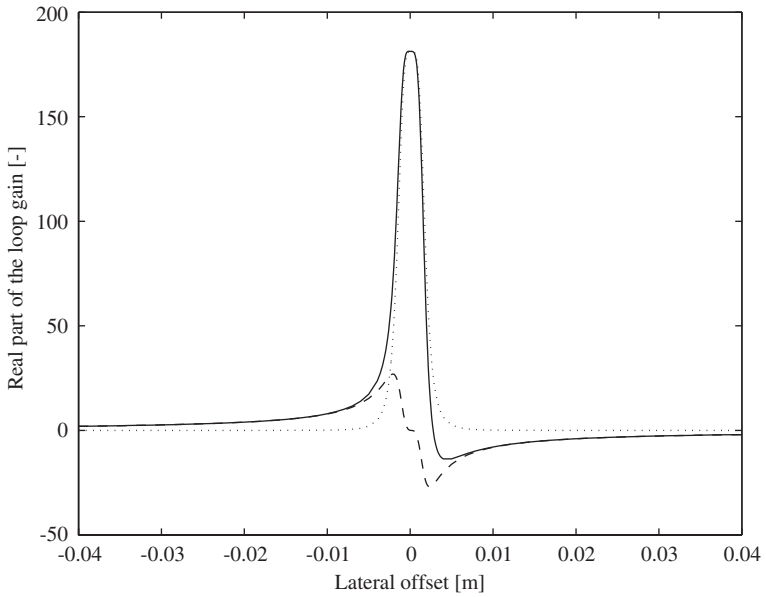

Fig. 13. Variation of the real parts of the transfer functions $H(\omega_{02})$ (solid line), $H_1(\omega_{02})$ (dashed line) and $H_2(\omega_{02})$ (dotted line) with the lateral offset u_{y+} for reference configuration.

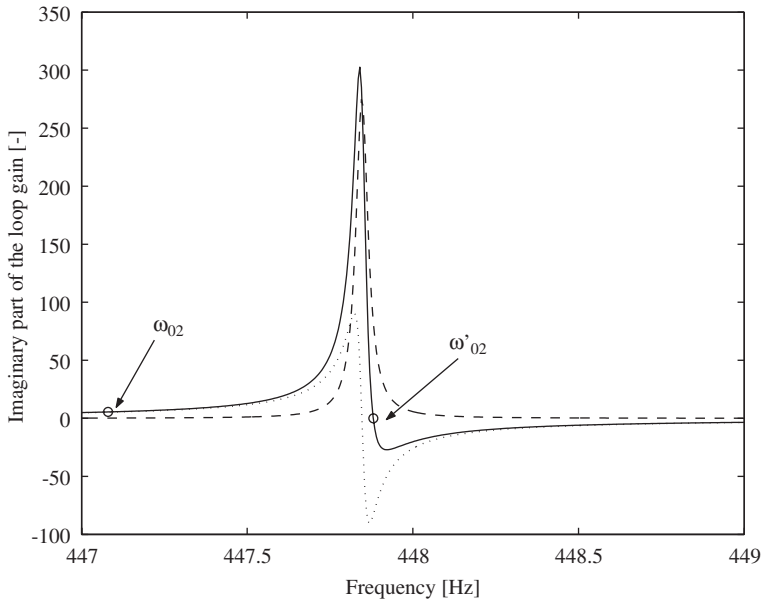

Fig. 14. Imaginary parts of the transfer functions $H(\omega)$ (solid line), $H_1(\omega)$ (dashed line) and $H_2(\omega)$ (dotted line) around ω_{02} for reference configuration but $u_{y+} = 0.01$ m.

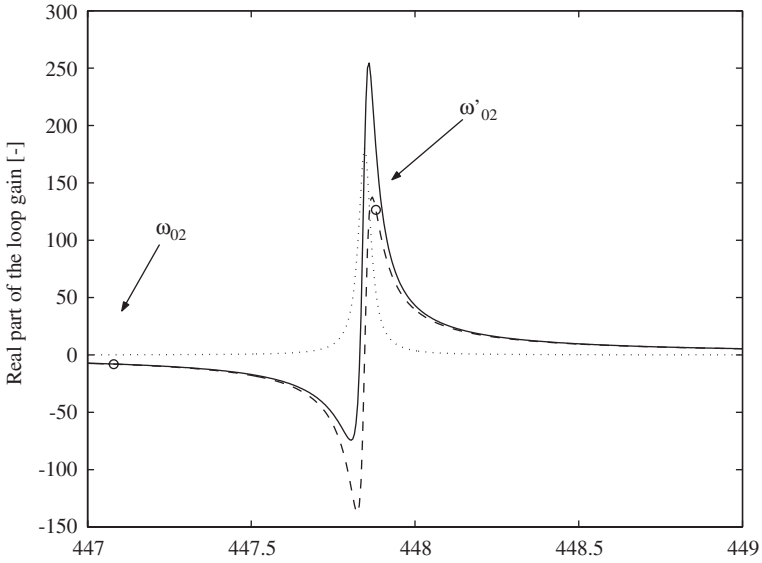

Fig. 15. Real parts of the transfer functions $H(\omega)$ (solid line), $H_1(\omega)$ (dashed line) and $H_2(\omega)$ (dotted line) around ω_{02} for reference configuration but $u_{y+} = 0.01$ m.

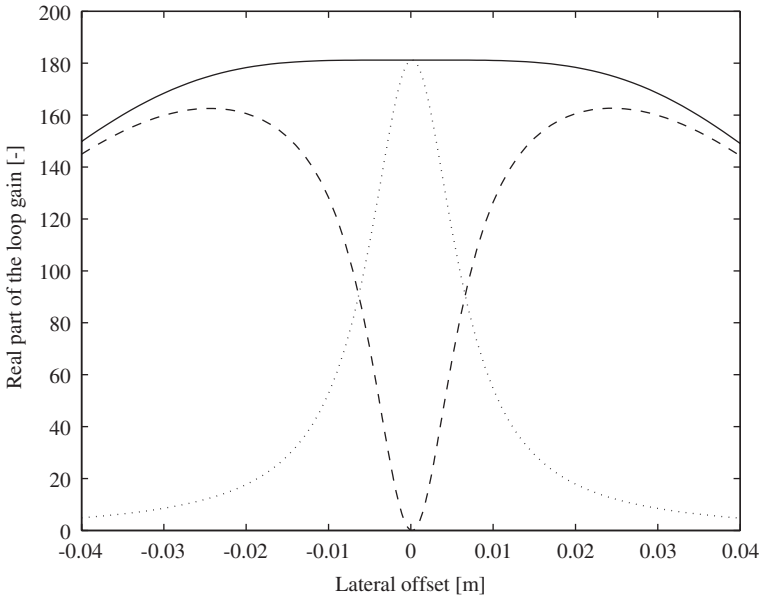

Fig. 16. Variation of the real parts of the transfer functions $H(\omega'_{02})$ (solid line), $H_1(\omega'_{02})$ (dashed line) and $H_2(\omega'_{02})$ (dotted line) with the lateral offset u_{y+} for reference configuration.

B.3. Zoom on the loop gain around the natural frequency of the mode

However, from Figs. 14 and 15, it can be noted that:

- $\Im(H)$ does not change polarity exactly at the natural frequency ω_{02},
- $\Re(H_1)$ rapidly changes polarity around this frequency.

Hence, in order to properly determine the stability of the mode, it is important to estimate the real part of the transfer functions at the frequency ω'_{02} where $\Im(H) = 0$.

In the case where $\gamma = 0$ (constant friction coefficient), it is also interesting to note that $c_{yy} \simeq 0$ in the saturated regimen. Hence, $H_2 = 0$ and $\Im(H) = \Im(H_1)$. Now, $\Im(H_1)$ does not change polarity around ω_{02} (see Fig. 14). Consequently, instability cannot occur with a constant friction coefficient, which corroborates the results given in Section 4.2.

B.4. Loop gain at the frequency where $\Im(H) = 0$

The variation of the real parts of the transfer functions $H(\omega'_{02})$, $H_1(\omega'_{02})$ and $H_2(\omega'_{02})$ with the lateral offset u_{y+} are given in Fig. 16 (note that ω'_{02} also depends on the lateral offset u_{y+}). This time, the results are very different from those given in Ref. [17]. In particular, $\Re(H_1)$ does not change polarity. Consequently, $\Re(H) > 1$ for all lateral offsets and the system is always unstable, which agrees well with the results of Section 4.2.

References

[1] N. Vincent, J.-R. Koch, H. Chollet, J.-Y. Guerder, Curve squeal of urban rolling stock—Part 1: State-of-the-art and field measurements, *Journal of Sound and Vibration*, this issue (doi:10.1016/j.jsv.2005.12.008).

[2] J.-R. Koch, N. Vincent, H. Chollet, O. Chiello, Curve squeal of urban rolling stock—Part 2: Parameter study on a 1/4 scale rig, *Journal of Sound and Vibration*, this issue (doi:10.1016/j.jsv.2005.12.009).

[3] M.J. Rudd, Wheel/rail noise, part II: wheel squeal, *Journal of Sound and Vibration* 46 (3) (1976) 395–417.

[4] M. Nakai, Y. Chiba, M. Yokoi, Railway wheel squeal (1st report, on frequency of squeal), *Bulletin of the JSME* 25 (205) (1982) 1127–1134.

[5] M. Nakai, Y. Chiba, M. Yokoi, Railway wheel squeal (2nd report, mechanism of specific squeal frequency), *Bulletin of the JSME* 27 (224) (1984) 301–308.

[6] P.J. Remington, Wheel/rail squeal and impact noise: what do we know? What don't we know? Where do we go from here? *Journal of Sound and Vibration* 116 (2) (1985) 339–353.

[7] M. Nakai, M. Yokoi, Railway wheel squeal (3rd report, squeal of a disk simulating a wheel in internal resonances), *Bulletin of the JSME* 28 (237) (1985) 500–507.

[8] C.J.M. Van Ruiten, Mechanism of squeal noise generated by trams, *Journal of Sound and Vibration* 120 (2) (1988) 245–253.

[9] E. Schneider, K. Popp, H. Irretier, Noise generation in railway wheels due to rail-wheel contact forces, *Journal of Sound and Vibration* 120 (2) (1988) 227–244.

[10] M. Nakai, M. Yokoi, M. Sugiura, Railway wheel squeal (squeal of a rotating disk), *JSME International Journal, Series III* 32 (3) (1989) 406–412.

[11] U. Fingberg, A model of wheel-rail squealing noise, *Journal of Sound and Vibration* 143 (3) (1990) 365–377.

[12] F. Périard, Curve Squeal Noise by Trams, Ph.D. Thesis, Delft University of Technology, Netherlands, 1995.

[13] M. Nakai, S. Akiyama, Railway wheel squeal (squeal of a disk subjected to periodic excitation), *Journal of Vibration and Acoustics* 120 (2) (1998) 614–622.

[14] M. Nakai, S. Akiyama, Railway wheel squeal (squeal of a disk subjected to random excitation), *JSME International Journal, Series C* 41 (3) (1998) 608–615.

[15] M.A. Heckl, I.D. Abrahams, Curve squeal of train wheels, part 1: mathematical model for its generation, *Journal of Sound and Vibration* 229 (3) (2000) 669–693.

[16] M.A. Heckl, Curve squeal of train weels, part 2: which wheel modes are prone to squeal? *Journal of Sound and Vibration* 229 (3) (2000) 695–707.

[17] F.G. de Beer, M.H.A. Janssens, P.P. Kooijman, Squeal noise of rail-bound vehicles influenced by lateral contact position, *Journal of Sound and Vibration* 267 (3) (2003) 497–507.

[18] J.T. Oden, J.A.C. Martins, Models and computational methods for dynamic friction phenomena, *Computer Methods in Applied Mechanics and Engineering* 52 (1985) 527–634.

[19] R.A. Ibrahim, Friction-induced vibration, chatter, squeal, and chaos, part II: dynamics and modelling, *Applied Mechanics Review* 47 (7) (1994) 227–253.

[20] A. Akay, Acoustics of friction, *Journal of the Acoustical Society of America* 111 (4) (2002) 1252–1548.

[21] K. Kraft, Der einfluß der fahrgeschwindigkeit auf den haftwert zwischen rad und schiene, *Archiv für Eisenbahntechnik* 22 (1967) 58–78.

[22] J.J. Kalker, Wheel-rail rolling contact theory, *Wear* 144 (1991) 243–261.

[23] K. Knothe, R. Wille, B.W. Zastrau, Advanced contact mechanics-road and rail, *Vehicle System Dynamics* 35 (4–5) (2001) 361–407.

[24] H. Chollet, Contact roue-rail: vérification expérimentale de la théorie de Kalker, Report 135, INRETS, Arcueil, France, 1990.

[25] K.L. Johnson, *Contact Mechanics*, Cambridge University Press, Cambridge, 1985.